

1 Study of tapered microfibers by line-field confocal optical coherence 2 tomography

3 **Arnaud Dubois, Aloïs Baudry, Sylvie Lebrun**

4 *Université Paris-Saclay, Institut d'Optique Graduate School, CNRS, Laboratoire Charles Fabry, 91127, Palaiseau, France*

5 *Corresponding author e-mail address: sylvie.lebrun@institutoptique.fr*

6

7 **Keywords:** silica microfibers, optical tapers, line-field confocal optical coherence tomography, silica
8 optical fibers

9 **Abstract**

10 We present for the first time to our knowledge measurements of the evolution of the core and cladding
11 diameters in tapered silica microfibers using LC-OCT. The results could help refine models of
12 propagation of optical modes in tapers.

13 **1. Introduction and motivations**

14 Optical microfibers are typically produced by tapering standard silica fibers—commonly used in
15 telecommunications—until their diameters become comparable to or smaller than the wavelength of the
16 propagating light. The uniform section of the resulting structure, referred to as the microfiber, is
17 connected to the untapered fiber parts through two conical sections known as tapers (see Figure 1).
18 These devices have been extensively used for over three decades in both scientific research and
19 engineering, serving as fundamental optical devices that are inherently compatible with all-fiber
20 networks [1]. Owing to their unique properties, microfiber-based technologies have proven to be
21 versatile across a wide range of applications, from fundamental studies to advanced implementations
22 such as quantum information systems [2,3], remote sensing devices [4], and nonlinear optics in the silica
23 itself [5,6] or in the surrounding medium via the evanescent field [7,8].

24 A key challenge in microfiber fabrication is ensuring the adiabaticity of the taper regions. An adiabatic
25 taper is characterized by a sufficiently small taper angle to suppress coupling between the guided
26 fundamental mode and unwanted higher-order modes, thereby preserving high transmission efficiency
27 of the desired mode. The standard adiabaticity criterion is based on the comparison of two characteristic
28 lengths. The first one is the beat length z_b between the fundamental LP_{01} mode and the nearest higher-
29 order mode with the same azimuthal symmetry, namely the LP_{02} mode. This beat length is obtained from
30 the difference between the longitudinal propagation constants of the two modes $\beta_{01}(z)$ and $\beta_{02}(z)$ along
31 the taper and is given by $z_b = \frac{2\pi}{\beta_{01}(z) - \beta_{02}(z)}$.

32 The second characteristic length is the local taper length z_t , which can be approximated as $z_t \approx \frac{\Omega(z)}{r(z)}$,
33 where $r(z)$ denotes the local cladding radius and $\Omega(z)$ the local taper angle [9]. When the condition

34 $z_t \gg z_b$ is satisfied at every position z along the taper - implying negligible intermodal coupling - the
35 taper can be considered adiabatic for the fundamental mode. Consequently, designing an adiabatic taper
36 profile requires calculating the propagation constants of the relevant modes throughout the taper as
37 functions of z , implying a precise knowledge of the refractive index profile.

38 In this study, we consider conventional step-index optical fibers consisting of a Ge:SiO₂-doped core
39 with refractive index n_{core} , surrounded by a pure SiO₂ cladding with refractive index n_{clad} . Current
40 theoretical models for the calculation of the propagation constants in such fibers rely on the following
41 assumptions: 1) the ratio between the cladding and core diameters remains constant throughout the taper;
42 2) the refractive indices of both the core and the cladding are uniform along the taper; 3) the core
43 effectively vanishes at a critical diameter, beyond which light guidance transitions from the core-
44 cladding interface to the cladding-external medium interface. In general, for step-index
45 telecommunication fibers, the critical cladding diameter is typically calculated to be around 40 μm [9].

46 **Typically, to design optimized tapers, three steps should be considered: the decrease of the diameter**
47 **should be firstly sharp until reaching the critical diameter, then much smoother when passing this**
48 **diameter to limit the coupling with higher order modes, then sharp again. This highlights the importance**
49 **to determine also the position and the value of this diameter.**

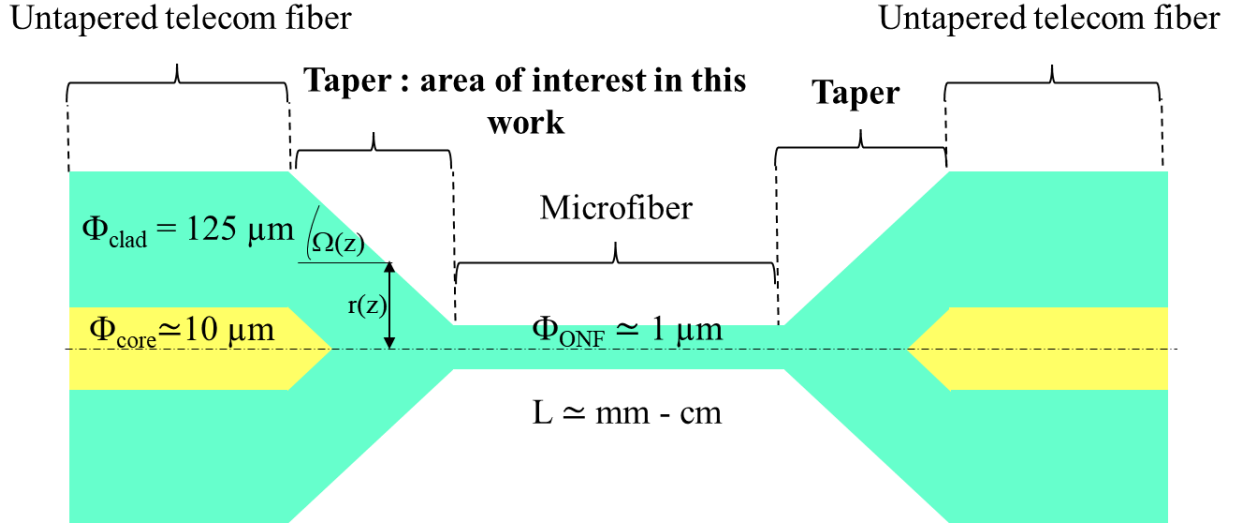
50 In this article, for the first time to our knowledge, we report on measurements of the tapered section of
51 a silica microfiber performed using Line-field Confocal Optical Coherence Tomography (LC-OCT),
52 aiming to assess the validity of the existing models.

53 Observing the evolution of both the core and cladding over distances of a few centimeters with high
54 resolution and sensitivity requires sophisticated techniques tailored to semi-transparent media.
55 Compared with nano- and microtomography methods, which offer higher sensitivity [10], LC-OCT
56 provides significantly faster acquisition times (on the order of tens of minutes to scan a ~ 2 cm-long
57 taper). Moreover, LC-OCT enables microscale characterization of macroscopic objects, whereas the
58 above-mentioned methods are typically limited to lengths of only a few millimeters. Quantitative phase
59 microscopy can also be used to obtain phase maps of the taper; however, unlike the approach presented
60 here, the resulting images are not directly amenable to physical interpretation [11]. Altogether, these
61 advantages make LC-OCT a complementary and powerful technique for investigating the evolution of
62 the core and cladding in the tapered section of a microfiber, with a micrometer-scale resolution and high
63 detection sensitivity.

64 This article is organized as follows:

65 After describing the experimental setup, we report results obtained from two different tapered sections
66 fabricated from step-index fibers designed for telecommunications (Alcatel Clear Incolore and Corning
67 SMF28e). Our measurements show that the assumptions commonly made for numerical modelling need
68 to be refined for a more accurate description of the evolution of propagation modes in the tapered
69 section.

70



71

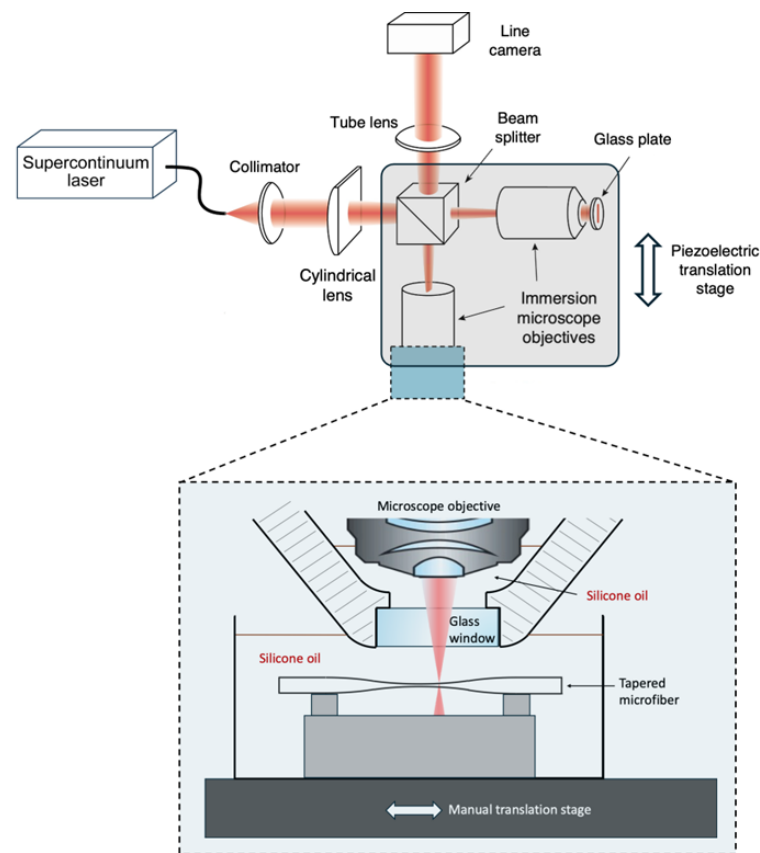
72 *Figure 1. Schematic diagram of a microfiber and its two tapers linking the uniform part to the untapered fiber. Φ_{clad} and*
 73 *Φ_{core} denote the cladding and core diameters, respectively, as indicated here for conventional single-mode step-index*
 74 *fibers used in telecommunications.*

75 2. Experimental setup

76 Line-field Confocal Optical Coherence Tomography (LC-OCT) is an optical imaging technique that
 77 combines confocal detection with low-coherence interferometry to provide real-time, cross-sectional
 78 images of semi-transparent samples [12]. The LC-OCT system used in this work, shown schematically
 79 in Figure 2, is routinely employed for cellular-level skin imaging [13,14]. Micrometer-scale lateral and
 80 axial resolution is achieved using two identical high numerical aperture (0.5) immersion microscope
 81 objectives and broadband light with a central wavelength of 750 nm. Illumination is provided by a fiber-
 82 coupled supercontinuum light source, whose output is collimated and shaped into a line by a cylindrical
 83 lens before entering the interferometer via a beam splitter. The line of light is focused onto the sample
 84 in the object arm of the interferometer and onto a glass plate in the reference arm. The interference signal
 85 is detected by a line-scan camera, and a vertical cross-sectional image is reconstructed from a stack of
 86 lines acquired by the camera as the depth is scanned using a piezoelectric translation stage [12,14]. The
 87 refractive index step $\Delta n = n_{\text{core}} - n_{\text{clad}}$ between the fiber core and the cladding being very small
 88 (typically a few 10^{-3}), the resulting optical reflection to be detected is very weak ($\sim 10^{-5}$). To enhance
 89 the interferometric signal contrast and thereby improve detection sensitivity, the reflection coefficient
 90 of the interferometer reference surface was reduced to 0.03% by immersing it in water.

91 The microfibers are drawn using the classical pull-and-brush technique with a butane flame, producing
 92 high-optical-quality microfibers with symmetrical tapers **in a very reproducible manner as was shown**
 93 **in previous studies** [6,7,15]. Two silica step-index single-mode fibers designed for telecommunications
 94 are studied (Alcatel Clear Incolore and Corning SMF28e, respectively named fiber 1 and fiber 2). The
 95 initial cladding diameter of both fibers is 125 μm . The characteristics of fiber 2 are well-known. Its
 96 initial core diameter is 8.2 μm , and its step-index is $\Delta n = 5.2 \times 10^{-3}$ [11]. Although the parameters of

97 fiber 1 (diameters and step-index) are less well characterized, they are known to be similar. In both
 98 cases, the targeted microfiber diameter is $1.71 \mu\text{m}$. The length of the uniform part of the microfibers is
 99 1 cm, and the length of the tapers is 1.8 cm. **The microfiber and its two tapers are immersed in a tank**
 100 **filled with silicone oil (refractive index ≈ 1.45) to attenuate optical reflections at the fiber surface (see**
 101 **Figure 2). Consequently, the contrast in optical reflection between the cladding surface and the core**
 102 **surface is reduced.** A series of cross-sectional LC-OCT images of the taper is acquired at positions
 103 separated by 0.5 mm. **Each cross-sectional image is generated by averaging 100 frames to reduce photon**
 104 **shot noise. The device is mechanically stable, ensuring that this averaging does not introduce blur that**
 105 **could degrade spatial resolution.**



106

107 *Figure 2. LC-OCT setup. The tapered microfiber under study is not shown to scale and is enlarged for illustration*
 108 *purposes.*

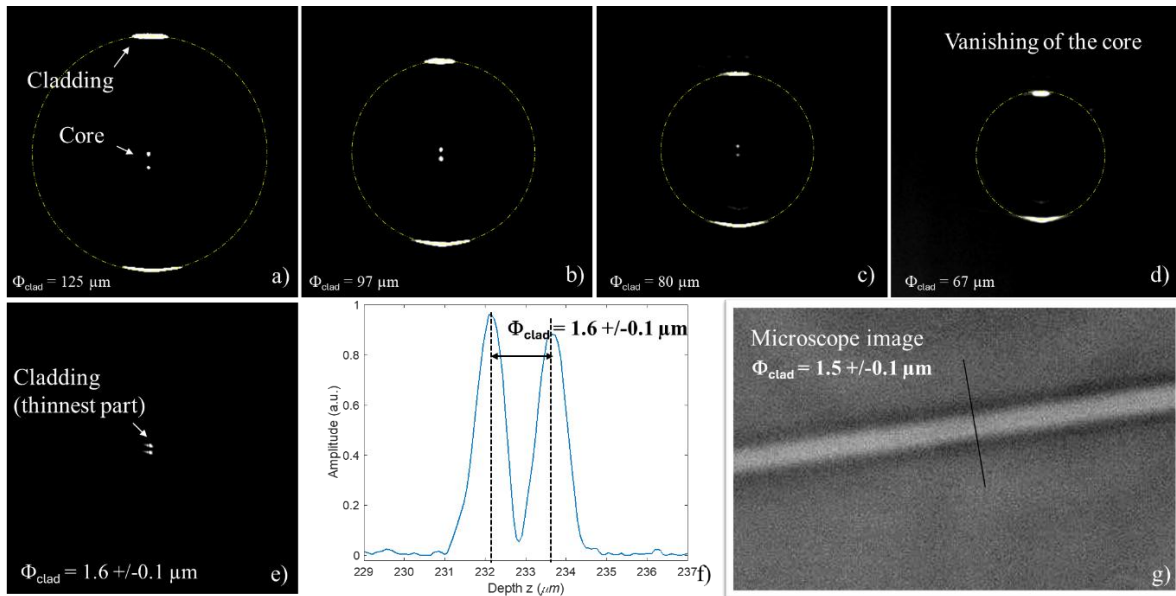
109

110 3. Results and discussion

111 Figures 3(a)-(e) show cross-sectional images of the tapered section of fiber 1 for different cladding
 112 diameters. The white traces indicate the cladding, and the small points at the center of the images in
 113 Figures 3(a)-(c) indicate the core. **Because the cladding and core surfaces are smooth, the optical**
 114 **reflection is predominantly specular. Only light reflected from surface regions that are nearly**
 115 **perpendicular to the illumination direction is detected. Fitting the visible cladding boundary in the image**
 116 **with a circle confirms its circular geometry, although only a portion of it is observed. From the initial**

117 diameter of 125 μm down to a cladding diameter of approximately 67 μm , the cladding/core interface
 118 could still be observed despite the small step index. The resolution of the LC-OCT device enabled to
 119 measure the diameter of the thinnest part, namely the microfiber (Figures 3(e) and 3(f)), yielding a
 120 diameter value of 1.6 μm +/- 0.1 μm . This measurement is in very good agreement with the value
 121 obtained by conventional optical microscopy using an immersion microscope objective (see Figure
 122 3(g)), giving a diameter of 1.5 μm +/-0.1 μm . Both measurements are also in good agreement with the
 123 targeted diameter of 1.71 μm . **Performing measurements by Scanning Electron Microscopy (SEM)**
 124 **provides much higher resolution but is far more complex to implement than this optical method.**
 125 **Moreover, in our previous works, we have performed SEM measurements that have shown that our**
 126 **drawing machine yields very good results in terms of diameter accuracy and homogeneity [7,15].**

127 In Figure 4(a), we report the evolution of the cladding and core diameters along the taper. As the
 128 diameters decrease, the reflectivities also decrease due to the progressive diffusion of the Ge:SiO₂ core
 129 during the tapering process, leading to a reduction of the step index value. In particular, the smallest
 130 core diameter that could be measured is 1.85 μm for a cladding diameter of 67 μm . Below this value,
 131 the detection limit of LC-OCT is reached [12], corresponding to a minimum reflectivity $R_{min} =$
 132 $\left(\frac{\Delta n}{n_{core}+n_{clad}}\right)^2 \approx 10^{-9}$, which is obtained for a refractive-index step of $\Delta n \approx 10^{-4}$.



133

Figure 3. From a) to e) Cross-sectional images of the tapered section of fiber 1 for 5 different cladding diameters (125 μm , 97 μm , 80 μm , 67 μm and 1.6 μm). The yellow dotted lines represent a fit of the external boundary of the fiber with a circle f) Measurement of the thinnest part diameter obtained by LC-OCT. g) Optical microscopy image of the thinnest part of the fiber.

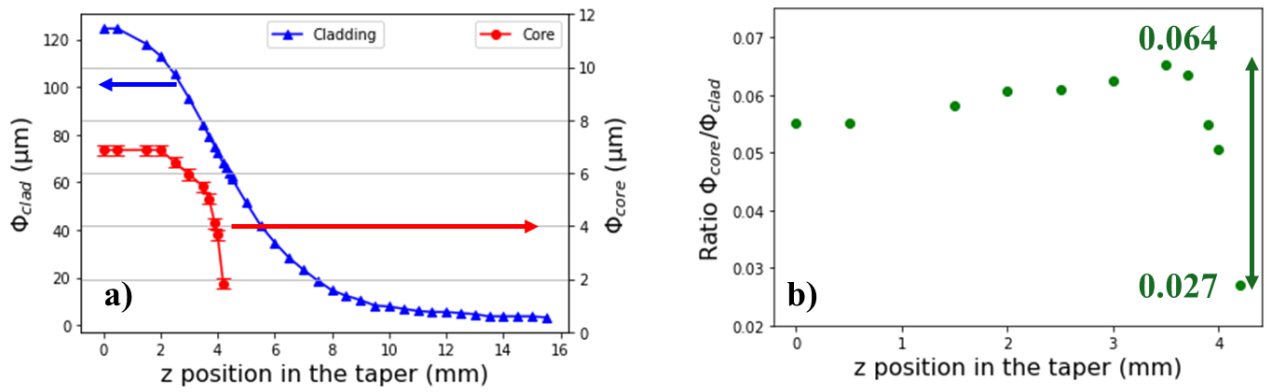


Figure 4. a) Evolution of the cladding (blue triangles) and core diameters (red dots) versus the z position in the taper drawn from fiber 1. Error bars on Φ_{core} are $\pm 0.1 \mu\text{m}$ (smaller than the size of the cladding marks). b) Evolution of the ratio of the core and cladding diameter $R = \Phi_{core}/\Phi_{clad}$ versus the z position in the taper in the area where the core diameter is measurable. Error bars are smaller than the size of the marks ($\pm 0.1\%$).

134

135 In Figure 4 (b), we plot the ratio of the core to cladding diameters, $R = \frac{\Phi_{core}}{\Phi_{clad}}$. This ratio is not constant,
 136 varying from 0.064 to 0.05 over the first 4.5 millimeters in the taper. It then decreases abruptly to 0.027
 137 for the last point that could be measured. ~~We believe that this apparently random variation arises from~~
 138 ~~the combined effects of the taper and microfiber fabrication processes, as well as from inhomogeneities~~
 139 ~~in the core of the untapered fiber. Further investigations are required to fully understand this behavior.~~

140 Our hypothesis is that there are two distinct effects occurring during the tapering process : the geometrical
 141 reduction of the initial core size and the expansion of the region of higher refractive index, due to the
 142 diffusion of Ge into the cladding in the vicinity of the initial core. We still name this region 'core'. These
 143 two combined effects could explain the behavior observed in Figure 4b, that can be separated into three
 144 parts :

- 145 - At the beginning, until $z = 2.5$ mm, the increase in core size due to diffusion is negligible
 146 compared to the reduction in core size from the fiber stretching, giving an almost constant ratio
 147 R .
- 148 - After $z = 2.5$ mm, there is a more pronounced increase in the ratio R until $z = 3.5$ mm because
 149 of a more important diffusion reducing the core diameter decrease speed.

150 Then after $z = 3.5$ mm, R decreases sharply because of both the reduction of the geometrical size of the
 151 core and the fact that the index difference Δn is flattened due to diffusion and becomes lower than the
 152 detection limit.

153 The same measurements were performed with a taper drawn from fiber 2. The results are shown in
 154 Figure 5.

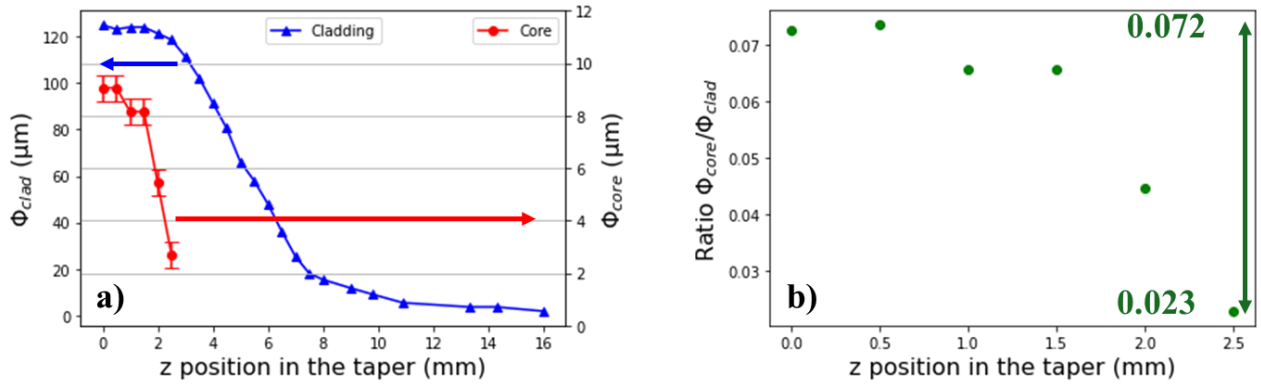


Figure 5. a) Evolution of the cladding (blue triangles) and core diameters (red dots) versus the z position in the taper drawn from fiber 2. Error bars on Φ_{core} are $\pm 0.5 \mu\text{m}$ (smaller than the size of the cladding marks). b) Evolution of the ratio of the core and cladding diameter Φ_{core}/Φ_{clad} versus the z position in the taper in the area where the core diameter is measurable. Error bars are smaller than the size of the marks ($\pm 0.1\%$).

155

156 Even for large cladding diameters, the core was more difficult to observe than for fiber 1, which we
 157 attribute to a smaller initial step index. The step index for the untapered fiber 2 being known ($\Delta n =$
 158 5.2×10^{-3}), we deduce that the step index of untapered fiber 1 should be higher. Determining its exact
 159 value would require a calibration of the LC-OCT system, which we were not able to do for practical
 160 reasons. As for fiber 1, the vanishing of the core corresponds to the limit of detection of the LC-OCT
 161 device. We conclude that the range of variation of the step index we were able to measure for fiber 2
 162 extends from 5.2×10^{-3} to $\sim 10^{-4}$. In Figure 5 (a), the core vanishes for a cladding diameter of 91 μm ,
 163 and the smallest core diameter that could be measured is 2.7 μm . The smallest cladding diameter
 164 measured is 1.8 μm , in good agreement with the targeted diameter of 1.71 μm . In Figure 5 (b), we report
 165 the ratio of the core and cladding diameters. As for fiber 1, this ratio decreases, from 0.072 to 0.023. **The**
 166 **decrease appears more monotonic than for fiber 1, with a two step behavior without any increase of the**
 167 **ratio R, suggesting that the diffusion of Ge does not counter balance the effect of the geometrical**
 168 **reduction of the core size. Further investigations based on measurement of the chemical composition of**
 169 **the taper (synchrotron or X-rays for instance) would be necessary to confirm this assumption. Moreover,**
 170 fewer data points were acquired, which prevents a definitive comparison. **Similar measurements were**
 171 **performed on 3 identical microfibers drawn from fiber 1 and 2 from fiber 2, showing the same results.**

172 4. Conclusion and perspectives

173 To our knowledge, we report for the first time measurements of the evolution of the cladding and core
 174 diameters along the tapered section of a microfiber fabricated using the classical pull-and-brush
 175 technique, obtained by LC-OCT. This imaging technique is particularly attractive, as it does not require
 176 complex preparation of the samples and enables fast high-sensitivity measurements with micrometer-
 177 scale resolution of semi-transparent objects such as silica tapers.

178 The results show that, contrary to assumptions commonly used in numerical models, the ratio of the
 179 core to cladding diameters is not constant along the taper. We attribute this behavior to both the fiber

180 origin and the fabrication process. Moreover, the step-index is found to decrease, at least down to a value
181 of $\sim 10^{-4}$, corresponding to the detection limit of LC-OCT. At last, for both fibers, we measured that
182 the critical diameter is not obtained for a diameter of 40 μm as currently used but depends on the single
183 mode fiber: for fiber 1, this diameter is 67 μm whereas for fiber 2, it is 91 μm . These results can be used
184 to optimize the shape of the tapers and to calculate more precisely the effective index of the propagation
185 mode in the taper.

186 Future work will focus on collecting additional data to obtain reliable statistics and on investigating
187 other types of optical fibers (*e.g.* polarization-maintaining fiber, visible single-mode fibers, fibers with
188 other silica dopings, ...). These results will enable the refinement of numerical models of mode
189 propagation in tapers, particularly for the design and optimization of adiabatic taper profiles.

190

191 **References**

192 [1] Tong LM et al., Subwavelength-diameter silica wires for low-loss optical wave guiding, *Nature* 426,
193 816 – 819 (2003) DOI: 10.1038/nature02193

194 [2] Berroir J et al., Ultralow-power single-pass all-optical photon router, *Optica* 12 (8), pp. 1250-51
195 (2025). <https://doi.org/10.1364/OPTICA.569736>

196 [3] Horikawa S et al., Low-loss telecom-band nanofiber cavity for interfacing Yb atomic qubits, *Opt.*
197 *Lett.* 50 (17), pp. 5294-98 (2025) DOI:10.1364/OL.570362

198 [4] Zhang L, et al., Micro-/Nanofiber Optics: Merging Photonics and Material Science on Nanoscale for
199 Advanced Sensing Technology, *iScience* 23(1), 100810 (2020). DOI:10.1016/j.isci.2019.100810

200 [5] Birks TA, et al., Supercontinuum generation in tapered fibers, *Opt Lett.* 2000 Oct 1;25(19):1415-7.
201 doi: 10.1364/ol.25.001415. PMID: 18066233.

202 [6] Delaye P, et al., Continuous-wave generation of photon pairs in silica nanofibers using single-
203 longitudinal and multilongitudinal-mode pumps, *Phys Rev A* 104, 063715 (2021). DOI:
204 10.1103/PhysRevA.104.063715 DOI: <https://doi.org/10.1103/PhysRevA.104.063715>

205 [7] Bouhadida M et al., Highly efficient and reproducible evanescent Raman converters based on a silica
206 nanofiber immersed in a liquid, *Appl. Phys. B* 125, 228 (2019). DOI:10.1007/s00340-019-7340-7

207 [8] Fanjoux G et al., Demonstration of the evanescent Kerr effect in optical nano fibers, *Opt. Express*
208 27, 29460 – 29470 (2019). doi: 10.1364/OE.27.029460

209 [9] Love JD et al., *IEE Proc. Pt.J: Optoelectronics*, vol. 138 (5), pp. 343-354, 1991.
210 <https://doi.org/10.1049/ip-j.1991.0061>

211 [10] Crocco MC et al., Multiscale X-ray computed tomography of standard optical fibers, *Tomography*
212 *of Materials and Structures* 9:100078, Nov. 2025 DOI:10.1016/j.tmater.2025.100078

213 [11] Belanger E et al., Comparative study of quantitative phase imaging techniques for refractometry of
214 optical waveguides, *Optics Express*, vol 26 (13), p. 17498 (2018) DOI:10.1364/OE.26.017498

215 [12] Dubois A et al., Line-field confocal time-domain optical coherence tomography with dynamic
216 focusing, *Opt. Express* 26, 33534-33542 (2018). DOI: 10.1364/OE.26.033534

217 [13] Dubois A et al, Line-field confocal optical coherence tomography for high-resolution noninvasive
218 imaging of skin tumors, *J. Biomed. Opt.* 23, 106007 (2018). DOI: 10.1117/1.JBO.23.10.106007

219 [14] Latriglia F et al., Line-Field Confocal Optical Coherence Tomography (LC-OCT) for Skin Imaging
220 in Dermatology, *Life*, vol. 13, pp. 2268 (2023). <https://doi.org/10.3390/life13122268>

221 [15] Shan L et al, Stimulated Raman scattering in the evanescent field of liquid immersed tapered
222 nanofibers, *Appl. Phys.Lett.* 102 (20), 201110 (2013) <https://doi.org/10.1063/1.4807170>

223

224

225

226 **Conflict of interests**

227 The authors declare that there are no conflicts of interest related to this article.

228 **Funding**

229 The work was supported by internal fundings.

230 **Data availability statement**

231 This article has no associated data generated.

232 **Author contribution statement**

233 A. Dubois and S. Lebrun collected and processed the data and wrote the article. A. Baudry and S. Lebrun
234 fabricated the nanofibers. A. Dubois, A. Baudry and S. Lebrun discussed the results and reviewed the
235 article.

236